

Highly spin-polarized carriers and strong ferromagnetism in doped perovskite antiferromagnetic semiconductors

Hong Jian Zhao,^{1,2,3,4} Longju Yu,¹ Yanchao Wang,^{1,3,*} Laurent Bellaiche,⁵ and Yanming Ma^{1,4,3,†}

¹Key Laboratory of Material Simulation Methods and Software of Ministry of Education, College of Physics, Jilin University, Changchun 130012, China

²Key Laboratory of Physics and Technology for Advanced Batteries (Ministry of Education), College of Physics, Jilin University, Changchun 130012, China

³State Key Laboratory of Superhard Materials, College of Physics, Jilin University, Changchun 130012, China

⁴International Center of Future Science, Jilin University, Changchun 130012, China

⁵Physics Department and Institute for Nanoscience and Engineering, University of Arkansas, Fayetteville, Arkansas 72701, USA

(Dated: June 9, 2023)

In semiconductor spintronics, the generation of highly spin-polarized carriers and the efficient probe of spin order (due to strong ferromagnetism) – at or above room temperature – are crucial because it allows for the design of spin-based semiconductor devices. Usually, such goals were fulfilled in room-temperature ferromagnetic semiconductors, being rare materials in nature. While room-temperature antiferromagnetic semiconductors are plentiful, the possibility for creating highly spin-polarized carriers and strong ferromagnetism in these materials remain to be unraveled. Here, we explore such a possibility by first-principles simulations, working with CaTcO_3 and NaOsO_3 perovskites – being room-temperature antiferromagnetic semiconductors. We find that doping them by electrons or holes results in these materials to be highly spin-polarized, carrying enormous ferromagnetic moments. Doping electrons with moderate carrier density can yield strong ferromagnetism in them, with the ferromagnetic moments being comparable to that in typical ferromagnetic semiconductors. Our work thus indicates the merit of perovskite antiferromagnetic semiconductors in spintronics – for a possible replacement of ferromagnetic semiconductors.

Introduction. – Ferromagnetic semiconductors are of vital significance in semiconductor spintronics [1–4]. Materials of this kind present giant Zeeman-type spin splittings and strong ferromagnetism, where the former allow for the generation of highly spin-polarized carriers and the latter permits the efficient probe of spin order [1, 2, 5]. One shortcoming of ferromagnetic semiconductors is that the Curie temperatures of these materials are usually far lower than room temperature [1, 6], making the ferromagnetic semiconductors lose their practical applications. In this regard, ferrimagnetic semiconductors and related materials – such as asymmetric and bipolar antiferromagnetic semiconductors [7], being still rare at room temperature – may come to the rescue, serving as the “weak version” of ferromagnets (see, *e.g.*, Refs. [4, 6, 8–10]). On the other hand, there are a variety of perovskite semiconductors being antiferromagnetic with Néel temperatures being above room temperature [11, 12]. Some of these perovskites (*e.g.*, YFeO_3 and CaTcO_3) can host Zeeman-type spin splittings and weak ferromagnetism [13, 14]. Typically, the Zeeman-type spin splitting can reach ~ 78 meV in CaTcO_3 perovskite [14], being sizable – albeit a tiny value compared with ~ 2 eV in YTiO_3 [15]; The magnitudes of magnetic moments in antiferromagnets are much smaller than those in ferromagnets (*e.g.*, $\sim 0.06 \mu_B/f.u.$ in antiferromagnetic YFeO_3 [13] *versus* $\sim 0.8 \mu_B/f.u.$ in ferromagnetic YTiO_3 [16, 17]). At all events, this suggests a route to utilize perovskite antiferromagnetic semiconductors as alternatives for ferromagnetic semiconductors in spin-

tronics, if the following questions are positively answered: (i) Is it possible to generate highly spin-polarized carriers in antiferromagnetic semiconductors? (ii) Is there an avenue to realize strong ferromagnetism in antiferromagnetic semiconductors?

In this Letter, we address the aforementioned questions by first-principles simulations. We focus on perovskite CaTcO_3 and NaOsO_3 , whose Néel temperatures are ~ 800 K [18] and ~ 410 K [19–22], respectively. Below Néel temperatures, these materials are all antiferromagnetic semiconductors [19–24]. We show that doping CaTcO_3 and NaOsO_3 by electrons or holes leads them to be highly spin-polarized, due to the sizable Zeeman-type spin splittings of energy levels around their valence band maximum (VBM) and conduction band minimum (CBM). The doped carriers, carrying enormous ferromagnetic moments, significantly enhance the ferromagnetism in antiferromagnetic CaTcO_3 and NaOsO_3 . In particular, doping electrons with the carrier density of 0.125 *e/f.u.* (*e* being the charge of electron) gives rise to ferromagnetic moments of $\sim 0.3 \mu_B/f.u.$ in CaTcO_3 and $\sim 0.2 \mu_B/f.u.$ in NaOsO_3 , an order of magnitude being comparable to those in perovskite ferromagnetic semiconductors (*e.g.*, $\sim 0.8 \mu_B/f.u.$ in YTiO_3 [16, 17]).

Spin splittings versus spin-polarized carriers. – To begin with, we revisit the possibilities for creating spin-polarized carriers in semiconductors by doping. In centrosymmetric non-magnetic semiconductors, the electron’s spin energy levels associated with $+S_\alpha$ and $-S_\alpha$ ($\alpha = x, y, z$), the spin magnetization of the electron,

are degenerate everywhere in \mathbf{k} space (\mathbf{k} being the wave vector). Doping such semiconductors is not expected to yield spin-polarized carriers because the carriers occupy $+S_\alpha$ and $-S_\alpha$ states in a symmetrical manner [see Fig. 1(a)]. As for the non-centrosymmetric non-magnetic semiconductors, a \mathbf{k} -dependent effective magnetic field $\mathbf{B}^{\text{eff}}(\mathbf{k})$ is emerged because of the spin-orbit coupling (SOC) [25, 26]. Such a field couples with electron's spin via $\mathbf{B}^{\text{eff}}(\mathbf{k}) \cdot \boldsymbol{\sigma}$ [25] and yields, *e.g.*, Rashba-/Dresselhaus-type spin splittings [27, 28], where $\boldsymbol{\sigma} \equiv (\sigma_x, \sigma_y, \sigma_z)$ is the vector formed by Pauli matrix σ_α ($\alpha = x, y, z$). In other words, the $+S_\alpha$ and $-S_\alpha$ levels become non-degenerate at some non-zero \mathbf{k} [see Fig. 1(b)]. Nonetheless, the lack of magnetism indicates the odd-function feature of $\mathbf{B}^{\text{eff}}(\mathbf{k})$, namely, $\mathbf{B}^{\text{eff}}(-\mathbf{k}) = -\mathbf{B}^{\text{eff}}(\mathbf{k})$ [25]; As a consequence, each $\pm S_\alpha$ state at any wave vector \mathbf{k} can find its degenerate partner (*i.e.*, $\mp S_\alpha$ state) at the corresponding $-\mathbf{k}$. In such sense, the doped carriers are not spin-polarized either in non-centrosymmetric non-magnetic semiconductors [see Fig. 1(b)].

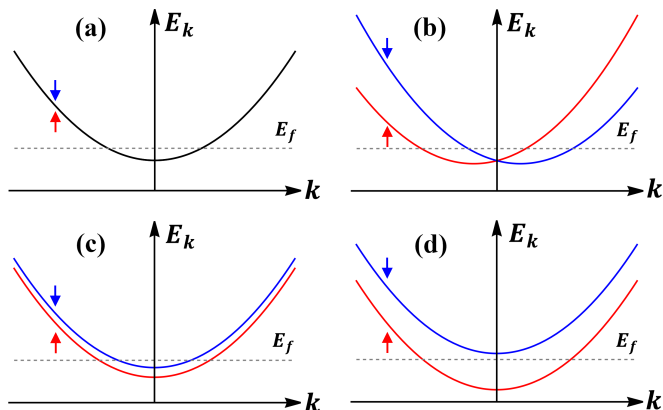


FIG. 1. Schematizations of the band structures (*i.e.*, band energies E_k versus the wave vector \mathbf{k}) in electron-doped semiconductors with null spin splitting [panel (a)], Rashba-/Dresselhaus-type spin splitting [panel (b)], tiny Zeeman-type spin splitting [panel (c)], and sizable Zeeman-type spin splitting [panel (d)]. The split energy levels with positive and negative spin magnetization values are sketched in red and blue curves (and marked by red and blue arrows), respectively. The horizontal dash line in each panel denotes the Fermi energy level E_f .

In ferromagnetic or ferrimagnetic materials, there exists an effective magnetic field B_α^{eff} being independent of \mathbf{k} . The interaction between B_α^{eff} field and electron's spin, indicated by $B_\alpha^{\text{eff}} \sigma_\alpha$, causes Zeeman-type spin splittings in these materials [2, 29]. If so, the degeneracy between $+S_\alpha$ and $-S_\alpha$ state (α being a particular direction determined by B_α^{eff}) can be broken by the B_α^{eff} effective magnetic field [see Fig. 1(d)]. Recent studies indicate that some antiferromagnetic semiconductors showcase weak ferromagnetism together with Zeeman-type spin splittings (see, *e.g.*, Ref. [14, 30, 31]). In such sense, the

doped carriers in antiferromagnetic semiconductors occupy the $+S_\alpha$ and $-S_\alpha$ states asymmetrically and thus can be spin-polarized [32, 33]. Antiferromagnetic semiconductors with tiny Zeeman-type spin splittings around the CBM (VBM) [34] gain doped electrons (holes) that are slightly spin-polarized [Fig. 1(c)], while semiconductors with sizable Zeeman-type splittings yield carriers being significantly (even 100%) spin-polarized [Fig. 1(d)]. Provided that the Zeeman-type spin splittings are large enough around the VBM or CBM, the doped carriers may carry sizable ferromagnetic moment – reinforcing the weak ferromagnetism in antiferromagnetic semiconductors.

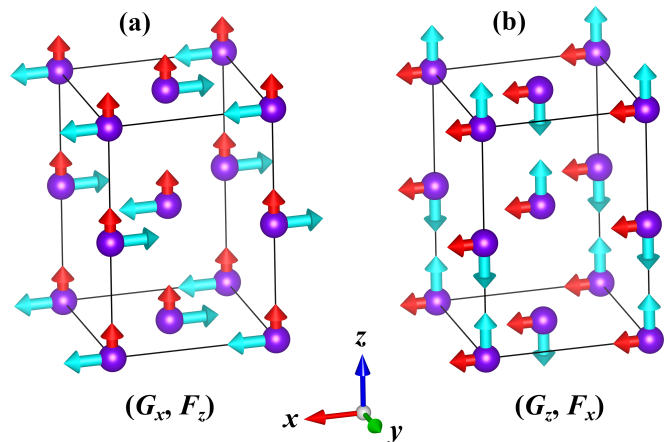


FIG. 2. Schematizations of the (G_x, F_z) and (G_z, F_x) magnetic configurations in $Pbnm$ ABX_3 perovskite. In panels (a) and (b), the predominant G -type and the weak F -type vectors (carried by B ions – represented by purple spheres) are denoted by cyan and red arrows, respectively. For displaying clarity, the A and X ions are not shown in the schematizations.

Doped perovskite antiferromagnets: the spin-polarized carriers. – In the following, we will demonstrate that our aforementioned scenario can be realized in antiferromagnetic ABX_3 perovskites. We recall that various ABX_3 perovskites (*e.g.*, rare-earth orthoferrites [11, 35], rare-earth orthochromates [11, 36], SrTcO_3 [37], CaTcO_3 [18] and NaOsO_3 [19, 20]) adopt the $Pbnm$ crystallographic space group with the predominant G -type antiferromagnetic vectors carried by B ions. Symmetry analyses and experiments [11, 35, 36, 38, 39] indicate that two magnetic configurations – termed as (G_x, F_z) and (G_z, F_x) magnetic configurations and sketched in Fig. 2 – can present weak ferromagnetism (due to spin canting) in $Pbnm$ perovskite with G -type antiferromagnetism. To be specific, aligning the predominant G -type vectors along x direction (denoted by G_x) causes weak ferromagnetic vectors along z (*i.e.*, being F -type and denoted by F_z). Similarly, the predominant G_z antiferromagnetic vectors yield the weak ferromagnetic F_x vectors. Theories suggest that (G_x, F_z) and (G_z, F_x) magnetic configurations

accommodate Zeeman-type spin splittings that are microscopically rooted in SOC, where the magnitudes of Zeeman-type spin splittings depend on the strength of SOC [14]. The split spin energy levels are associated with spin magnetization $\pm S_z$ for (G_x, F_z) configuration and $\pm S_x$ for (G_z, F_x) configuration.

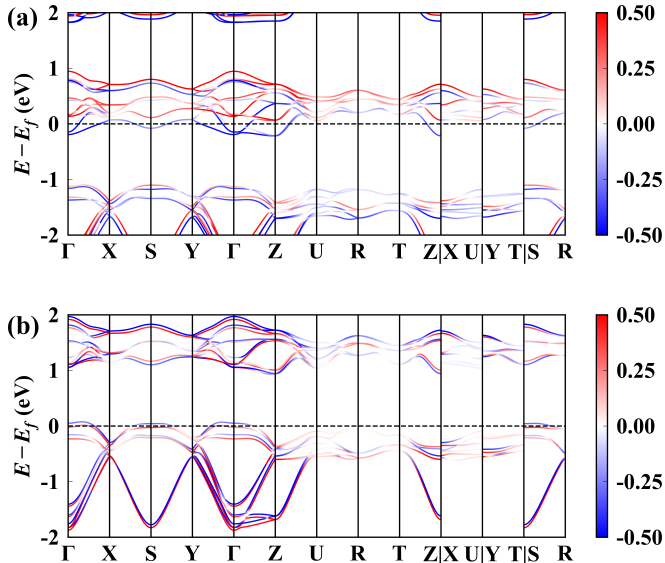


FIG. 3. The band structures of CaTcO₃ with the (G_x, F_z) magnetic configuration. The zero energy is set as the Fermi level E_f . Panels (a) and (b) correspond to electron ($n_{free} = +0.125 e/f.u.$) and hole ($n_{free} = -0.125 e/f.u.$) dopings, respectively. The color bar denotes the spin magnetization $\pm S_z$ (positive value for $+S_z$ and negative value for $-S_z$). In the horizontal axis, the \mathbf{k} -points in the high-symmetry path are represented by the reduced coordinates, with respect to the reciprocal lattice vectors.

Next, we select NaOsO₃, CaTcO₃ and YFeO₃ antiferromagnetic perovskites (G -type) as our platforms, where NaOsO₃ exhibits strong SOC, CaTcO₃ moderate SOC, and YFeO₃ weak SOC. We calculate the band structures of these materials with respect to (G_x, F_z) and (G_z, F_x) magnetic configurations, upon carrier doping (carrier density n_{free} being $\pm 0.125 e/f.u.$) – the positive and negative n_{free} values corresponding to electron and hole dopings, respectively. The band structures of CaTcO₃ with (G_x, F_z) magnetic configuration are shown in Fig. 3. Sizable Zeeman-type spin splittings occur around the CBM (respectively, VBM) of CaTcO₃ doped with electrons (respectively, holes). Upon electron doping, the extra electrons predominantly occupy the $-S_z$ states with tiny concentration occupying $+S_z$ states [Fig. 3(a)]. As a consequence, the $-S_z$ spin-polarized electrons are injected into the material. The hole doping in CaTcO₃ [with (G_x, F_z) configuration], similarly, creates holes that mostly occupy the $-S_z$ states, yielding $-S_z$ spin-polarized holes. Moving to the (G_z, F_x) configuration, the situations regarding Zeeman-

type spin splittings are similar to those in (G_x, F_z) configuration, as shown in Fig. S1 of the Supplementary Material (SM) [40] (Note that our SM contains Refs. [41–60]). In the (G_z, F_x) configuration of CaTcO₃, the doped electrons or holes prefer occupying the $+S_x$ states rather than the $-S_x$ states.

Our above discussion is basically valid for NaOsO₃ with (G_x, F_z) and (G_z, F_x) magnetic configurations (see Fig. S2 of the SM). By saying “*basically*” we mean that (i) the carriers in NaOsO₃ predominantly occupy the $\pm S_\alpha$ level [e.g., $\alpha = z$ in (G_x, F_z) configuration or $\alpha = x$ in (G_z, F_x)] – resembling the cases in CaTcO₃, and (ii) a small amount of carriers may also occupy $\mp S_\alpha$ level – the partner of the $\pm S_\alpha$ level. In such sense, the carriers in NaOsO₃ are partially spin-polarized. As for YFeO₃, the SOC is negligible and the Zeeman-type spin splittings are tiny. Figure S3 in the SM indicates that the spin magnetization $|S_\alpha|$ in the vicinity of the doping level [$\alpha = z$ for (G_x, F_z) and $\alpha = x$ for (G_z, F_x)] is almost vanishing. Furthermore, the doped carriers occupy $+S_\alpha$ and $-S_\alpha$ states in a nearly symmetrical manner (see Fig. S4 of the SM). Hence, the spin polarization of the doped carriers in YFeO₃ is rather insignificant.

Doped perovskite antiferromagnets: the enhanced ferromagnetism. – In the undoped $Pbnm$ NaOsO₃, CaTcO₃ and YFeO₃, the predominant G -type antiferromagnetic vectors tend to align along the x axis (compared with y and z axes), as predicted by our first-principles calculations. This yields the (G_x, F_z) magnetic configuration in these materials and coincides with the experiments (see e.g., Refs. [13, 18, 20] and Section I of the SM). Furthermore, the calculated magnetic moments (M_z, M_x) for NaOsO₃, CaTcO₃ and YFeO₃ are $(0.016, -0.003)$, $(0.057, -0.059)$ and $(0.066, -0.063)$ $\mu_B/f.u.$, respectively, with (i) M_z being associated with F_z in the (G_x, F_z) configuration, and (ii) M_x being associated with F_x in the (G_z, F_x) configuration [61].

We now explore the effect of carrier doping on ferromagnetism in these perovskite antiferromagnets. First of all, our first-principles calculations, at the level of collinear magnetism, show that the G -type magnetic phase in NaOsO₃, CaTcO₃ and YFeO₃ are more stable upon doping with $n_{free} = \pm 0.125 e/f.u.$, compared with the A -, C -, and F -type magnetic phases (see Section III of the SM). That NaOsO₃ becomes a G -type antiferromagnetic metal upon electron doping is basically consistent with the results shown in Refs. [62, 63]. In the following, our discussion will be limited within the (G_x, F_z) and (G_z, F_x) magnetic configurations.

Figure 4(a) shows the M_z – in the (G_x, F_z) magnetic configuration – of CaTcO₃, NaOsO₃ and YFeO₃ as a function of n_{free} . In CaTcO₃, doping electrons (holes) reinforces its ferromagnetic component along the $-z$ direction ($+z$ direction). This can be interpreted in the following way. As shown in Fig. 3(a), the doped electrons are $-S_z$ polarized (see above) which carries the

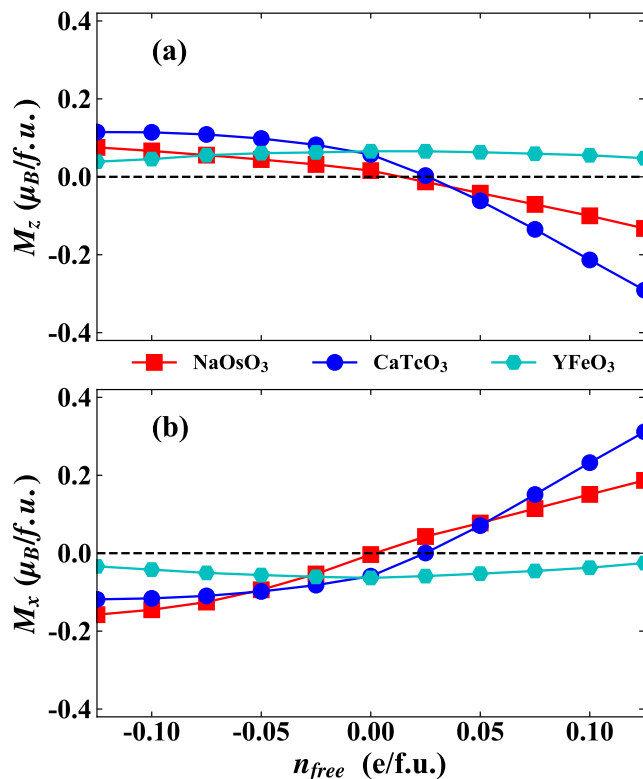


FIG. 4. The magnetic moments of CaTcO₃, NaOsO₃ and YFeO₃ as a function of carrier density n_{free} . Panels (a) and (b) correspond to the (G_x, F_z) and (G_z, F_x) magnetic configurations, respectively.

ferromagnetic moments along $-z$ direction. As for hole doping, the holes are $-S_z$ polarized as well; Yet, the hole doping is equivalent to removing electrons from the $-S_x$ states of CaTcO₃, creating the ferromagnetic moments along $+z$ direction. Regarding the (G_z, F_x) configuration of CaTcO₃, the doping effect on ferromagnetism is readily understood by examining Fig. 4(b) and Fig. S1 of the SM. Furthermore, the trends for the magnetic moments of NaOsO₃ (versus n_{free}) follow those of CaTcO₃. The physical interpretation is akin to the case of CaTcO₃ (see Fig. S2 of the SM). Unlike CaTcO₃ and NaOsO₃, the magnetic moments of YFeO₃ remain inert upon carrier doping for both (G_x, F_z) and (G_z, F_x) magnetic configurations (see Fig. 4). This results from the insignificant spin polarization of the doped carriers in YFeO₃, and coincides with our discussion in the Section “*Doped perovskite antiferromagnets: the spin-polarized carriers*”.

To finish this section, we emphasize that carrier doping can significantly enhance the ferromagnetism in antiferromagnetic CaTcO₃ and NaOsO₃. Strikingly, doping CaTcO₃ with electrons ($n_{free} = +0.125$ e/f.u.) yields ferromagnetic moment of the order of ~ 0.3 $\mu_B/f.u.$ in both (G_x, F_z) and (G_z, F_x) magnetic configurations. As for NaOsO₃, doping electrons with $n_{free} = +0.125$ e/f.u.

results in M_x of ~ 0.2 $\mu_B/f.u.$ in the (G_z, F_x) configuration. Such ferromagnetic moments are comparable to those in the typical ferromagnetic perovskites (e.g., ~ 0.8 $\mu_B/f.u.$ in YTiO₃ [16, 17]). For CaTcO₃ and NaOsO₃, the electron doping level $n_{free} = 0.125$ e/f.u. corresponds to the volume concentrations of $\sim 2 \times 10^{21}$ cm³, a concentration that could be accessible by electrostatic doping (see, e.g., Refs. [64, 65]). Furthermore, we are aware of an avenue to realizing the electron doping in NaOsO₃ (i.e., via the replacement of Na with Mg), as proposed by Ref. [66] – focusing on the insulator-to-metal transition in NaOsO₃ driven by doping.

Summary and perspective. – By first-principles simulations, we have shown that CaTcO₃ and NaOsO₃ antiferromagnetic perovskites enable the creation of highly spin-polarized carriers by either electron doping or hole doping, thanks to the sizable Zeeman-type spin splittings of the electrons’ energy levels in the vicinity of CBM or VBM. The doped electrons or holes carry enormous ferromagnetic moments and significantly enhance the ferromagnetism in antiferromagnetic CaTcO₃ and NaOsO₃, compared to their undoped neutral cases. Promisingly, the Néel temperatures of CaTcO₃ and NaOsO₃ are all above the room temperature. This implies a route to (i) inject highly spin-polarized carriers (and generate spin current), and (ii) create sizable ferromagnetic moments in doped perovskite antiferromagnetic semiconductors, at room temperature and in the absence of magnetic field. As a perspective, it is possible to foresee the importance of room-temperature perovskite antiferromagnetic semiconductors – exhibiting sizable Zeeman-type spin splittings around their VBM and CBM – in spintronics. We hope that our work can motivate the utilization of such antiferromagnetic semiconductors in the design and fabrication of room-temperature spintronic devices.

Acknowledgements. – We acknowledge the support from the National Natural Science Foundation of China (Grants Nos. 12274174, T2225013, 52288102 and 12034009). L.B. thanks the Office of Naval Research (ONR) under Grant No. N00014-17-1-2818 and the Vannevar Bush Faculty Fellowship (VBFF) Grant No. N00014-21-1-2086 from the Department of Defense. L.J.Y. acknowledges the support from the International Center of Future Science, Jilin University. The calculation was performed in the high-performance computing center of Jilin University. The authors thank Prof. P. Liu at Chinese Academy of Sciences (Institute of Metal Research) for the valuable discussion regarding the Hubbard U correction in NaOsO₃.

* wyc@calypso.cn

† mym@jlu.edu.cn

- [1] S. Wolf, D. Awschalom, R. Buhrman, J. Daughton, v. S. von Molnár, M. Roukes, A. Y. Chtchelkanova, and D. Treger, *Science* **294**, 1488 (2001).
- [2] J. Xia, W. Ge, and K. Chang, *Semiconductor Spintronics* (WORLD SCIENTIFIC, 2011).
- [3] Y. Huang, V. Polojärvi, S. Hiura, P. Höjer, A. Aho, R. Isoaho, T. Hakkarainen, M. Guina, S. Sato, J. Takayama, A. Murayama, I. A. Buyanova, and W. M. Chen, *Nat. Photonics* **15**, 475 (2021).
- [4] X. Li and J. Yang, *Natl. Sci. Rev.* **3**, 365 (2016).
- [5] P. Němec, M. Fiebig, T. Kampfrath, and A. V. Kimel, *Nat. Phys.* **14**, 229 (2018).
- [6] S. K. Kim, G. S. D. Beach, K.-J. Lee, T. Ono, T. Rasing, and H. Yang, *Nat. Mater.* **21**, 24 (2021).
- [7] The asymmetric antiferromagnetic semiconductors and bipolar antiferromagnetic semiconductors reported in Refs. [8, 10], being ferrimagnetic semiconductors in essence, involve more than one magnetic sublattice with almost cancelled magnetic moments. The densities of states of these materials (together with ferrimagnetic semiconductors) resemble those in ferromagnets, with giant splittings between spin-up and spin-down channels. Consequently, the doped carriers in these materials can be highly spin-polarized, significantly tuning the magnetic moments.
- [8] P. Wang, D. Wu, K. Zhang, and X. Wu, *J. Phys. Chem. Lett.* **13**, 3850 (2022).
- [9] Y.-m. Nie and X. Hu, *Phys. Rev. Lett.* **100**, 117203 (2008).
- [10] X. Li, X. Wu, Z. Li, and J. Yang, *Phys. Rev. B* **92**, 125202 (2015).
- [11] E. Bousquet and A. Cano, *J. Phys.: Condens. Matter* **28**, 123001 (2016).
- [12] V. Baltz, A. Manchon, M. Tsoi, T. Moriyama, T. Ono, and Y. Tserkovnyak, *Rev. Mod. Phys.* **90**, 015005 (2018).
- [13] J.-S. Zhou, L. G. Marshall, Z.-Y. Li, X. Li, and J.-M. He, *Phys. Rev. B* **102**, 104420 (2020).
- [14] X. Liu, H. J. Zhao, L. Bellaiche, and Y. Ma, Submitted (2023).
- [15] P. Liu, Y. Wang, H. J. Zhao, L. Bellaiche, and Y. Ma, *Phys. Rev. B* **105**, 054402 (2022).
- [16] H. D. Zhou and J. B. Goodenough, *J. Phys.: Condens. Matter* **17**, 7395 (2005).
- [17] A. S. Disa, J. Curtis, M. Fechner, A. Liu, A. von Hoegen, M. Först, T. F. Nova, P. Narang, A. Maljuk, A. V. Boris, B. Keimer, and A. Cavalleri, *Nature* **617**, 73 (2023).
- [18] M. Avdeev, G. J. Thorogood, M. L. Carter, B. J. Kennedy, J. Ting, D. J. Singh, and K. S. Wallwork, *J. Am. Chem. Soc.* **133**, 1654 (2011).
- [19] Y. G. Shi, Y. F. Guo, S. Yu, M. Arai, A. A. Belik, A. Sato, K. Yamaura, E. Takayama-Muromachi, H. F. Tian, H. X. Yang, J. Q. Li, T. Varga, J. F. Mitchell, and S. Okamoto, *Phys. Rev. B* **80**, 161104 (2009).
- [20] S. Calder, V. O. Garlea, D. F. McMorrow, M. D. Lumsden, M. B. Stone, J. C. Lang, J.-W. Kim, J. A. Schlueter, Y. G. Shi, K. Yamaura, Y. S. Sun, Y. Tsujimoto, and A. D. Christianson, *Phys. Rev. Lett.* **108**, 257209 (2012).
- [21] R. Sereika, P. Liu, B. Kim, S. Kim, J. Zhang, B. Chen, K. Yamaura, C. Park, C. Franchini, Y. Ding, and H. k. Mao, *npj Quantum Mater.* **5**, 66 (2020).
- [22] J. G. Vale, S. Calder, C. Donnerer, D. Pincini, Y. G. Shi, Y. Tsujimoto, K. Yamaura, M. M. Sala, J. van den Brink, A. D. Christianson, and D. F. McMorrow, *Phys. Rev. Lett.* **120**, 227203 (2018).
- [23] C. Franchini, T. Archer, J. He, X.-Q. Chen, A. Filippetti, and S. Sanvito, *Phys. Rev. B* **83**, 220402 (2011).
- [24] H. Wang, L. He, and X. Wu, *Comput. Mater. Sci.* **96**, 171 (2015).
- [25] L. L. Tao and E. Y. Tsymbal, *J. Phys. D: Appl. Phys.* **54**, 113001 (2021).
- [26] A. Manchon, H. C. Koo, J. Nitta, S. M. Frolov, and R. A. Duine, *Nat. Mater.* **14**, 871 (2015).
- [27] Y. A. Bychkov and E. I. Rashba, *JETP Lett.* **39**, 78 (1984).
- [28] G. Dresselhaus, *Phys. Rev.* **100**, 580 (1955).
- [29] T. Schäpers, *Semiconductor Spintronics* (De Gruyter, 2016).
- [30] L.-D. Yuan, Z. Wang, J.-W. Luo, and A. Zunger, *Phys. Rev. Mater.* **5**, 014409 (2021).
- [31] L.-D. Yuan, Z. Wang, J.-W. Luo, and A. Zunger, *Phys. Rev. B* **103**, 224410 (2021).
- [32] W. Dang, M. Zhu, Z. Zhu, X. Chen, Z. Song, and J. Qi, *Phys. Rev. Appl.* **18**, 064086 (2022).
- [33] H. J. Zhao, X. Liu, Y. Wang, Y. Yang, L. Bellaiche, and Y. Ma, *Phys. Rev. Lett.* **129**, 187602 (2022).
- [34] In semiconductors, electron doping or hole doping occurs around the CBM and VBM, respectively.
- [35] R. L. White, *J. Appl. Phys.* **40**, 1061 (1969).
- [36] B. Rajeswaran, D. I. Khomskii, A. K. Zvezdin, C. N. R. Rao, and A. Sundaresan, *Phys. Rev. B* **86**, 214409 (2012).
- [37] E. E. Rodriguez, F. Poineau, A. Llobet, B. J. Kennedy, M. Avdeev, G. J. Thorogood, M. L. Carter, R. Seshadri, D. J. Singh, and A. K. Cheetham, *Phys. Rev. Lett.* **106**, 067201 (2011).
- [38] L. Bellaiche, Z. Gui, and I. A. Kornev, *J. Phys.: Condens. Matter* **24**, 312201 (2012).
- [39] H. J. Zhao, P. Chen, S. Prosandeev, C. Paillard, K. Patel, J. Íñiguez, and L. Bellaiche, *Adv. Elect. Mater.* **8**, 2100639 (2021).
- [40] See Supplementary Material at [a link](#) for the methods used in the present work, and some numerical results regarding NaOsO₃, CaTcO₃ and YFeO₃.
- [41] G. Kresse and J. Furthmüller, *Phys. Rev. B* **54**, 11169 (1996).
- [42] G. Kresse and D. Joubert, *Phys. Rev. B* **59**, 1758 (1999).
- [43] P. E. Blöchl, *Phys. Rev. B* **50**, 17953 (1994).
- [44] D. M. Ceperley and B. J. Alder, *Phys. Rev. Lett.* **45**, 566 (1980).
- [45] S. L. Dudarev, G. A. Botton, S. Y. Savrasov, C. J. Humphreys, and A. P. Sutton, *Phys. Rev. B* **57**, 1505 (1998).
- [46] W. Zhang and P. Tong, *J. Phys.: Condens. Matter* **24**, 185401 (2012).
- [47] H. J. Zhao, L. Bellaiche, X. M. Chen, and J. Íñiguez, *Nat. Commun.* **8**, 14025 (2017).
- [48] K. Momma and F. Izumi, *J. Appl. Crystallogr.* **44**, 1272 (2011).
- [49] *SeeK-path* (<https://www.materialscloud.org/work/tools/seekpath>).
- [50] Y. Hinuma, G. Pizzi, Y. Kumagai, F. Oba, and I. Tanaka, *Comp. Mater. Sci.* **128**, 140 (2017).
- [51] A. Togo and I. Tanaka, *Spglib*: a software library for crystal symmetry search (2018), arXiv:1808.01590.
- [52] U. Herath, P. Tavazde, X. He, E. Bousquet, S. Singh, F. Munoz, and A. H. Romero, *Comput. Phys. Commun.* **251**, 107080 (2020).
- [53] *PYPROCAR* (<https://romerogroup.github.io/pyprocar/index.html>).
- [54] J. D. Hunter, *Comput. Sci. Eng.* **9**, 90 (2007).

- [55] *MAGNDATA* (<http://webbdcrystal1.ehu.es/magndata>).
- [56] S. V. Gallego, J. M. Perez-Mato, L. Elcoro, E. S. Tasci, R. M. Hanson, K. Momma, M. I. Aroyo, and G. Madariaga, *J. Appl. Crystallogr.* **49**, 1750 (2016).
- [57] S. V. Gallego, J. M. Perez-Mato, L. Elcoro, E. S. Tasci, R. M. Hanson, M. I. Aroyo, and G. Madariaga, *J. Appl. Crystallogr.* **49**, 1941 (2016).
- [58] S. Rye and M. J. Han, *J. Phys.: Condens. Matter* **30**, 275802 (2018).
- [59] E. Bousquet and N. Spaldin, *Phys. Rev. B* **82**, 220402 (2010).
- [60] P. Liu, J. He, B. Kim, S. Khmelevskiy, A. Toschi, G. Kresse, and C. Franchini, *Phys. Rev. Mater.* **4**, 045001 (2020).
- [61] The M_x and M_z are contributed by the both the spin and orbital magnetic moments.
- [62] S. K. Pandey, P. Mahadevan, and D. D. Sarma, *EPL* **117**, 57003 (2017).
- [63] S. Middey, S. Debnath, P. Mahadevan, and D. D. Sarma, *Phys. Rev. B* **89**, 134416 (2014).
- [64] K. Ueno, S. Nakamura, H. Shimotani, H. T. Yuan, N. Kimura, T. Nojima, H. Aoki, Y. Iwasa, and M. Kawasaki, *Nat. Nanotechnol.* **6**, 408 (2011).
- [65] J. Ma, R. Yang, and H. Chen, *Nat. Commun.* **12**, 2314 (2021).
- [66] S. Dobrovits, B. Kim, M. Reticcioli, A. Toschi, S. Khmelevskiy, and C. Franchini, *J. Phys.: Condens. Matter* **31**, 244002 (2019).